

Article

In Vitro Characterization of Doped Bioglass 45S5/HAp Coatings Obtained by CoBlast™ Deposition

Ana Sofia Pádua ^{1,2,†}, Sílvia Rodrigues Gavinho ^{3,*,†}, Tânia Vieira ², Imen Hammami ³,
Jorge Carvalho Silva ^{2,*}, João Paulo Borges ¹ and Manuel Pedro Fernandes Graça ³

- ¹ CENIMAT | i3N, Department of Materials Science, School of Science and Technology, NOVA University Lisbon, 2829-516 Caparica, Portugal; as.padua@campus.fct.unl.pt (A.S.P.); jpb@fct.unl.pt (J.P.B.)
² CENIMAT | i3N, Department of Physics, School of Science and Technology, NOVA University Lisbon, 2829-516 Caparica, Portugal; ts.vieira@fct.unl.pt
³ I3N and Physics Department, Aveiro University, 3810-193 Aveiro, Portugal; imenhammami@ua.pt (I.H.); mpfg@ua.pt (M.P.F.G.)
* Correspondence: silviagavinho@ua.pt (S.R.G.); jcs@fct.unl.pt (J.C.S.)
† These authors contributed equally to this work.

Abstract: Bone replacement is one of the major medical procedures in the oral surgery field due to the progressive ageing population and to illness or trauma in younger age groups. The use of implants without biological activity and effective osseointegration increases the chances of implant failure. This work aims to improve the interaction between implants and bone by using Bioglass 45S5 (BG)/hydroxyapatite (HAp) mixtures, including copper-, zinc-, and cerium-doped BG, as well as co-doping by the mentioned metals, as coatings produced by the CoBlast™ technique. All coatings present a uniform coverage of the Ti-6Al-4V substrate. Furthermore, in vitro testing using human osteosarcoma Saos-2 cells indicated that BG/HAp coatings have no cytotoxic effect, and the used of doping agents did not alter cell adhesion, proliferation, or alkaline phosphatase (ALP) expression when compared to undoped coating. These results demonstrate that BG/HAp by CoBlast™ can be a solution to improve implants' osseointegration.



Citation: Pádua, A.S.; Gavinho, S.R.; Vieira, T.; Hammami, I.; Silva, J.C.; Borges, J.P.; Graça, M.P.F. In Vitro Characterization of Doped Bioglass 45S5/HAp Coatings Obtained by CoBlast™ Deposition. *Coatings* **2023**, *13*, 1775. <https://doi.org/10.3390/coatings13101775>

Academic Editor: Oana Dragos-Pinzaru

Received: 10 September 2023
Revised: 5 October 2023
Accepted: 13 October 2023
Published: 16 October 2023



Copyright: © 2023 by the authors. Licensee MDPI, Basel, Switzerland. This article is an open access article distributed under the terms and conditions of the Creative Commons Attribution (CC BY) license (<https://creativecommons.org/licenses/by/4.0/>).

Keywords: CoBlast™; hydroxyapatite; Bioglass 45S5; copper; zinc; cerium; implant coating

1. Introduction

The field of medical implants has witnessed remarkable advancements in recent years, revolutionizing patient care by restoring functionality and improving quality of life. However, the successful integration of these implants within the complex biological system of the human body remains a challenge. Significant research efforts have been invested in implant surface modification to enhance biocompatibility, promote osseointegration, and mitigate potential complications such as biofilm-related infection [1–3]. In fact, implant surfaces, topography, and chemical composition have the greatest influence on the interaction between the biomaterial and bone tissue and, therefore, stability [4–8]. It is well-established that surface roughness, in particular, exhibits capacity in determining a biological response as roughness improves the processes and proliferation of osteoblasts and reduces the activity of osteoclasts, thus promoting the mineralization process [9–11]. In addition, implant roughness contributes to the process of the differentiation of mesenchymal cells towards the osteoblastic phenotype [10,12]. Several surface treatments/coatings have been studied and tested, such as particle blasting, laser processing, and plasma spray [13–16]. Although the coating processing methods are diverse, the CoBlast™ technique from ENBIO, Ireland, has been proven to be highly successful in the biomedical field [17–19]. This technique allows the metal's natural oxide layer removal by abrasion while also depositing the coating at room temperature. This method avoids the problems associated with other deposition techniques, especially problems related to a lack of mechanical stability and adhesion

to the substrate [1,17,20]. The Coblast™ process shows very promising characteristics and potential, allowing the achievement of a coating with significantly better mechanical properties, not only in terms of the coating/substrate adhesion, but also of the intra-coating cohesion, at a considerably lower cost.

It has been reported that the use of bioactive glass as a coating material can stimulate the good functioning of the implant due to its ability to enhance tissue integration and promote regeneration [21–24]. Based on the inorganic composition of natural bone, Hench et al. developed Bioglass®, which is capable of replacing damaged bone tissue without being rejected by the human body [23,25,26]. This reaction mechanism arises from the bioactive glass' ionic exchange capability within the surrounding physiological environment, enabling the migration of Ca^{2+} and PO_4^{3-} ions to the surface, forming an initial layer of amorphous calcium phosphate, which subsequently transforms into a crystalline hydroxyapatite layer. Several studies have reported that the insertion of inorganic ions such as copper, zinc, cerium, etc., into the glass network improves its biological response [27–29]. Trace elements play a crucial role in preserving overall health and preventing a variety of diseases. These essential elements are required in small amounts, but their effects on the body's physiological processes are profound. They contribute to enzymatic reactions, cellular functions, and structural integrity maintenance. Trace element deficiencies or imbalances can result in a variety of health problems such as weakened immune system function, impaired cognitive abilities, and bone diseases like osteoporosis [30,31]. One of these elements is copper (Cu), which plays a crucial role in promoting angiogenesis and facilitating the regeneration of both hard and soft tissues. Furthermore, Cu exhibits potential antibacterial properties due to its ability to generate reactive oxygen species (ROS), which can induce oxidative stress and damage bacterial cellular components [32,33]. Cerium (Ce) has garnered growing attention due to its ability to protect cells from damage caused by reactive oxygen species (ROS) and to reverse oxidative stress following implantation in bone, thereby promoting osteogenesis and expediting the bone healing process [34,35]. Zinc (Zn) has antimicrobial properties and significantly contributes to the proliferation of osteoblast cells and the stimulation of mineralization and bone formation by preventing the proliferation of bone-resorbing osteoclasts [36,37].

Although bioglass has achieved remarkable success, its high production cost has remained a significant issue. It has been reported that composite combining bioglass with calcium phosphate-based materials, such as hydroxyapatite (HAp) ($\text{Ca}_5(\text{PO}_4)_3(\text{OH})$), demonstrates enhanced biological properties compared to their individual phases, as reported in various studies [38,39]. Hydroxyapatite (synthetic or natural), which is the major inorganic component of human bones and teeth, has been used widely in orthopedic and dental applications, due to its excellent biocompatibility, and osteoconductive and osteoinductive properties [40–42]. The synergistic combination of bioglass and hydroxyapatite in coating applications induces rapid bone regeneration and functional integration, ultimately leading to improved clinical outcomes [38,43].

In this work, we attempt to demonstrate the potential of Bioglass 45S5/hydroxyapatite composite coatings using the CoBlast™ technique for application in both orthopedics and dental implants. For this purpose, bioglass modified by the doping and the co-doping of 2% mol Zn, 2% mol Ce, and 0.5% mol Cu was synthesized and subsequently mixed with the HAp. The selection of ion concentrations inserted in the bioglass is justified in our previous work [44–47]. The cytocompatibility of the coatings produced was assessed with the Saos-2 cell line. Moreover, cell adhesion and proliferation and alkaline phosphatase (ALP) activity were evaluated.

2. Materials and Methods

2.1. Materials Synthesis

The bioglass samples, based on the 45S5 formulation proposed by L. Hench (46.1SiO₂-2.6P₂O₅-24.35Na₂O-26.91CaO, mol%), were synthesized using the melt-quenching method. In this study, 7 types of samples were developed by adding several concentrations of

cerium, zinc, and copper oxides to the 45S5 base formulation [25]. All precursor reagents used were purchased from Sigma Aldrich, USA. The concentrations of each compound are described in Table 1.

Table 1. Molar percentages of each reagent in the different bioglass samples.

	Sample	Reagents (mol%)						
		SiO ₂	P ₂ O ₅	Na ₂ O	CaO	ZnO	CeO ₂	CuO
Doped	BG	46.10	2.60	24.35	26.91	-	-	-
	2Zn	45.18	2.55	23.86	26.37	2	-	-
	2Ce	45.18	2.55	23.86	26.37	-	2	-
	0.5Cu	45.87	2.59	24.25	26.78	-	-	0.5
	2Zn2Ce	44.26	2.49	23.38	25.83	2	2	-
Co-doped	2Zn0.5Cu	44.95	2.54	23.74	26.24	2	-	0.5
	2Ce 0.5Cu	44.95	2.54	23.74	26.24	-	2	0.5

Firstly, the high-purity SiO₂, Na₂CO₃, CaCO₃, and P₂O₅ starting materials that compose 45S5 (BG) were mixed in a ball mill system with agate vessels and balls for 1 h at 300 rpm. The mixed powders were calcined for 8 h at 800 °C in alumina crucibles. The oxides were added to calcinated BG and mixed at 300 rpm for 1 h. The several compositions were melted in a Pt crucible at 1300 °C for 1 h. The bioglass was re-melted to promote the homogeneity of the glass network. Quenching was carried out in a metal mold and the glass was subsequently ground. The glass was first ground in an agate mortar and then in a ball mill at 300 rpm for 1 h.

For the composites synthesis, all the bioglass compositions were mixed with hydroxyapatite (HAp) in the ball mill system at 200 rpm for 1 h, with the mass ratio shown in Table 2. The commercial hydroxyapatite used in the composites was supplied by Bioceramed, S.A., Portugal.

Table 2. Weight percentage of the bioglass and hydroxyapatite in the composite's samples.

Composites	Bioglass	HAp
BG/HAp		
2Zn/HAp		
2Ce/HAp		
0.5Cu/HAp	60	40
2Zn2Ce/HAp		
2Zn0.5Cu/HAp		
2Ce0.5Cu/HAp		

2.2. Coatings Synthesis

CoBlast™ was the method used to coat the metal substrates due to its room temperature conditions, the one-step surface preparation, and deposition process. Furthermore, this method is able to coat components with a variety of geometries [19,48].

Figure 1 shows the CoBlast™ equipment with a single nozzle configuration and Sulzer Metco's Single-10C powder feed system.

The substrates used in this study were Ti6Al4V grade 5 alloy (Jacquet, Ovar, Portugal) and had dimensions of 10 mm × 10 mm × 1 mm. Before deposition, the substrates were washed in 1 M HCl and then in acetone in an ultrasonic bath.

Since abrasion and powder deposition were carried out simultaneously, it was also necessary to add the abrasive in a 50/50 ratio to the composites. The abrasive used was Al₂O₃, also supplied by Bioceramed, S.A., Loures, Portugal.

Regarding the deposition conditions, the jet pressure was 4 bar, the distance between the nozzle and the substrate was 19 mm, and the nozzle was positioned at 90° to the substrates.

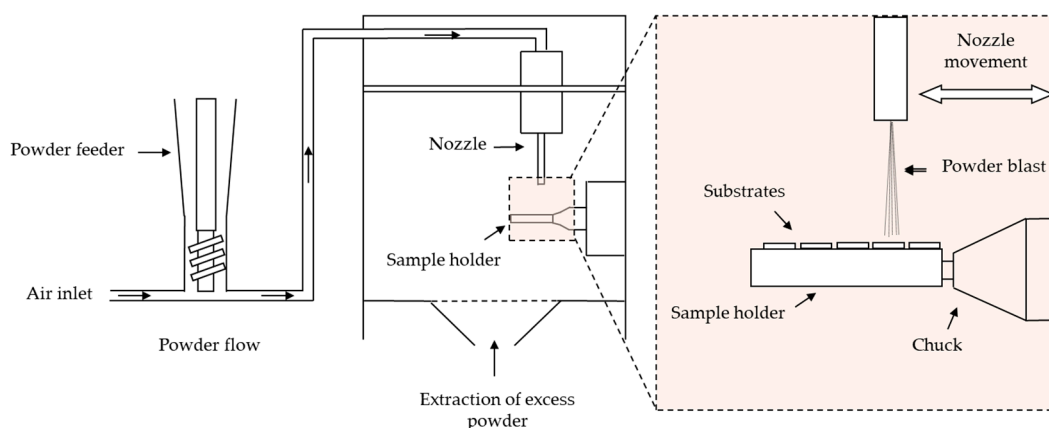


Figure 1. Schematic design of CoBlast™ equipment.

2.3. Morphological and Structural Characterizations

In this work, coating surface morphology was assessed by SEM (Scanning Electron Microscopy) using a TESCAN model Vega 3 (TESCAN ORSAY HOLDING, Brno, Czech Republic) microscope. The elemental analysis of the coating surface was also analyzed by Energy Dispersive X-ray Spectroscopy (EDS) using a Bruker QUANTAX detector (model XFlash MIN SVE) at 5 kV and 15 kV.

The powders used as coatings were analyzed by X-ray diffraction (XRD) at room temperature with an Aeris-Panalytical diffractometer with $\text{CuK}\alpha$ radiation ($\lambda = 1.54056 \text{ \AA}$) at 40 kV and 15 mA. The diffractograms were obtained in a 2θ range of 10° up to 70° and a scan step of 0.002° .

The coatings structure was analyzed by Grazing Incidence X-ray Diffraction (GIXRD) with $\text{CuK}\alpha$ radiation— 1.5406 \AA . The data were collected by a Rigaku SmartLab diffractometer at 40 kV and 30 mA. The patterns were obtained in the range of $10^\circ < 2\theta < 70^\circ$, scan speed of $0.6^\circ \text{ min}^{-1}$, and with an incident angle of 5° .

2.4. Cell Culture

2.4.1. Cytotoxicity Assay

A cytotoxicity assay was performed to compare cell viability of the different composite coatings using the extract method. Samples were sterilized at 120°C for 2 h. For extract preparation, sterilized samples were immersed in McCoy 5A culture medium with an exposed area of 1 cm^2 for each ml of medium and then incubated at 37°C for 48 h.

The human osteosarcoma Saos-2 cells were seeded at a concentration of 30 k cells/cm^2 and incubated for 24 h. Afterward, the medium was replaced by the extracts and 4 dilutions (corresponding to equivalent concentrations of $0.5 \text{ cm}^2/\text{mL}$, $0.25 \text{ cm}^2/\text{mL}$, $0.125 \text{ cm}^2/\text{mL}$, and $0.063 \text{ cm}^2/\text{mL}$), each with 6 replicates. For the resazurin test, two controls were set. The negative control, where cells were cultured in standard medium, a non-cytotoxic environment, and the positive control, where cells were cultured in a cytotoxic environment, created through the addition of 10% DMSO, a cytotoxic agent, to McCoy culture medium.

The sample extracts and cell controls were incubated for 48 h and afterward the extracts were replaced by a 50% McCoy and 50% resazurin solution that was incubated for 3 h. Cell activity was evaluated by determining the medium absorbance at 570 nm and 600 nm in a microplate reader (Biotek ELx 800UV, Winooski, VT, USA).

2.4.2. Adhesion and Proliferation

The sample ability to support cell metabolism was assessed through cell adhesion and proliferation studies. Samples were sterilized as previously described for the cytotoxicity assay.

The human osteosarcoma Saos-2 cells were seeded at a concentration of 20 k cells/cm^2 over the coating's surface and directly on the wells for the cell controls. Seeded cells were incubated at 37°C in a humidified 5% CO_2 atmosphere for 24 h in McCoy's medium.

Afterwards, cell adhesion rate was assessed using a resazurin absorbance. The resazurin assay was repeated at 3, 5, 7, and 9 days to follow cell proliferation behavior for all tested samples.

2.4.3. Alkaline Phosphatase Activity

ALP is an enzyme expressed by cells during osteogenesis, so it can be used as a differentiation marker. A colorimetric assay was used to evaluate ALP expression. This reaction used 1 mg/ml of 4-nitrophenyl phosphate disodium salt (Sigma-Aldrich, St. Louis, MO, USA) dissolved in tris-hydrochloric acid solution (pH 8.7). The first step in this assay consists of filtering the medium that was in contact with the samples, to remove any cell debris or dead cells. Then the absorbance at 405 nm was read to obtain the baseline. Next, the ALP solution was added in a 1:1 ratio to the medium and incubated for 30 min. Finally, the absorbance was measured at 405 nm.

The results were normalized to the populations determined on the previous day.

2.4.4. Immunofluorescence Study

For the immunofluorescence staining, the samples were fixed with paraformaldehyde for 20 min, washed with PBS, permeabilized using 0.5% Triton X-100 in PBS for 15 min, and washed again in PBS. Actin staining was carried out by incubating the cells in phalloidin conjugate (Phalloidin CruzFluor™ 488, Santa Cruz Biotechnology, Dallas, TX, USA) diluted in PBS in a 1:1000 ratio for 30 min in the dark and then the DNA was counterstained with 10 µg/mL DAPI for 5 min in the dark.

Actin and cell nuclei were observed using a Nikon Eclipse Ti-S fluorescence microscope equipped with a Nikon D610 digital camera. Images were obtained with a 40x objective.

2.4.5. Statistical Analysis

All data related to in vitro evaluation were statistically analyzed using the software OriginPro 2018 and presented using mean \pm SD. Furthermore, the statistical analysis was performed by one-way analysis of variance (One-way ANOVA) using Tukey's multiple comparison test. If the results presented $p < 0.05$, samples were accepted as significantly different.

3. Results

3.1. Morphological and Structural Characterizations

SEM micrographs were taken to assess the surface morphology. Figure 2 shows the surfaces of all the coatings obtained by CoBlast™ deposition.

All the samples have an identical morphology and show evidence of considerable roughness. The roughness caused by the abrasive allows for the tribochemical bonding and mechanical entrapment of the bioglass. The level of roughness promoted by this technique is also extremely useful for integrating implants into the bone [1,49].

Figure 3 shows the elemental analysis in mapping mode by EDS of the BG/HAp (a)–(f), 2Zn/HAp (g), 2Ce/HAp (h), and 0.5Cu/HAp (i) coatings. Figure 3a shows the presence of the alumina associated with the abrasive. The common elements of Bioglass 45S5 and hydroxyapatite (Ca and P) are presented in Figure 3c,d. The Si and Na presented in Figure 3e,f can distinguish Bioglass 45S5 from hydroxyapatite. The surface maps of the 2Zn/HAp, 2Ce/Hap, and 0.5Cu/HAp coatings were also produced, showing a homogeneous distribution of the additional elements in the Bioglass 45S5 network.

Figure 4 shows the diffractogram of the BG/Hap-coated sample using GIXRD. A significant contribution of Ti from the substrate and also the presence of alumina used as the abrasive is visible. Furthermore, it is possible to visualize the presence of hydroxyapatite. Bioglass, being an amorphous material, is not detected in the BG/HAp-coated sample.

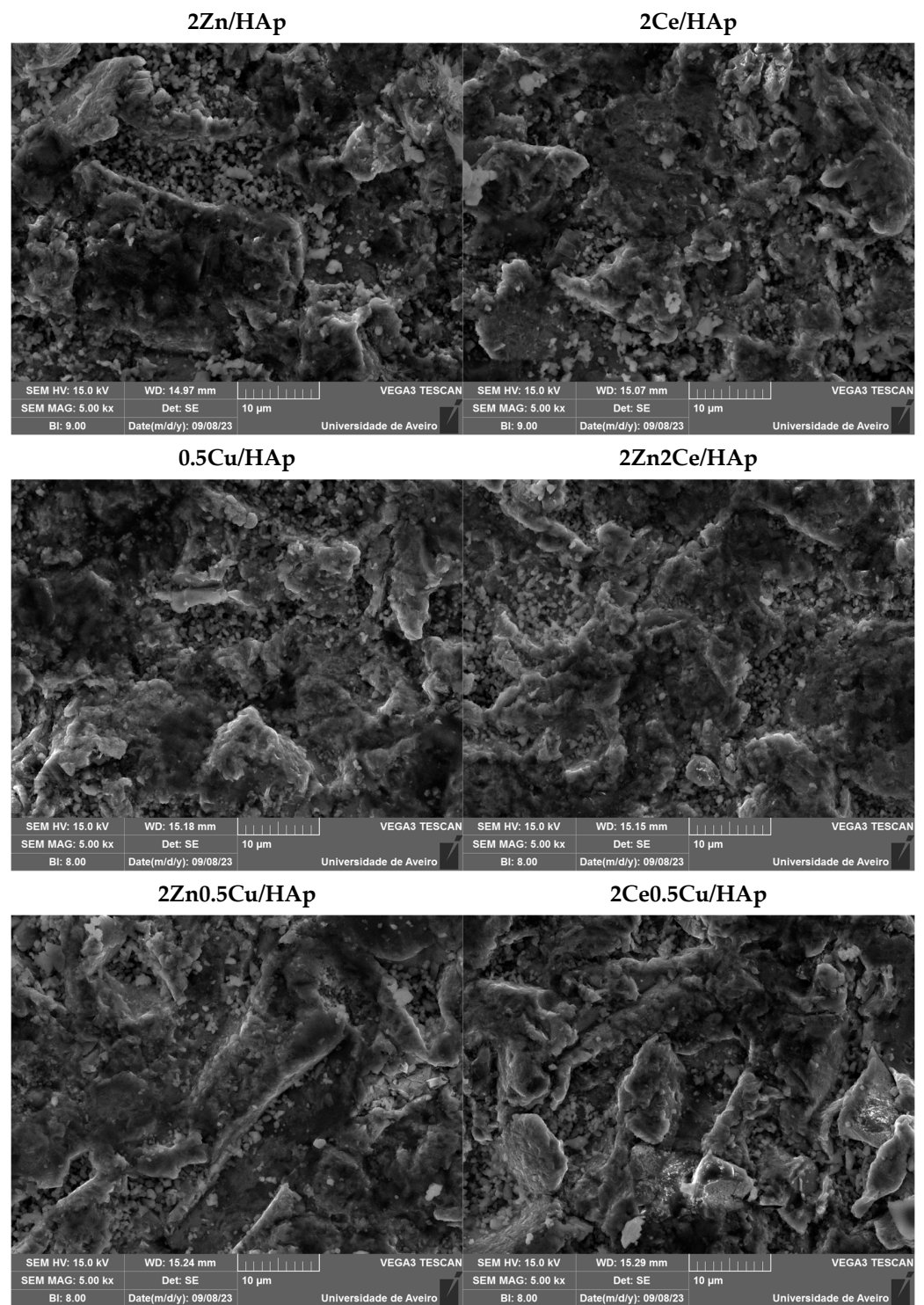


Figure 2. SEM micrographs of the coating surface (SEM magnification: 5kx).

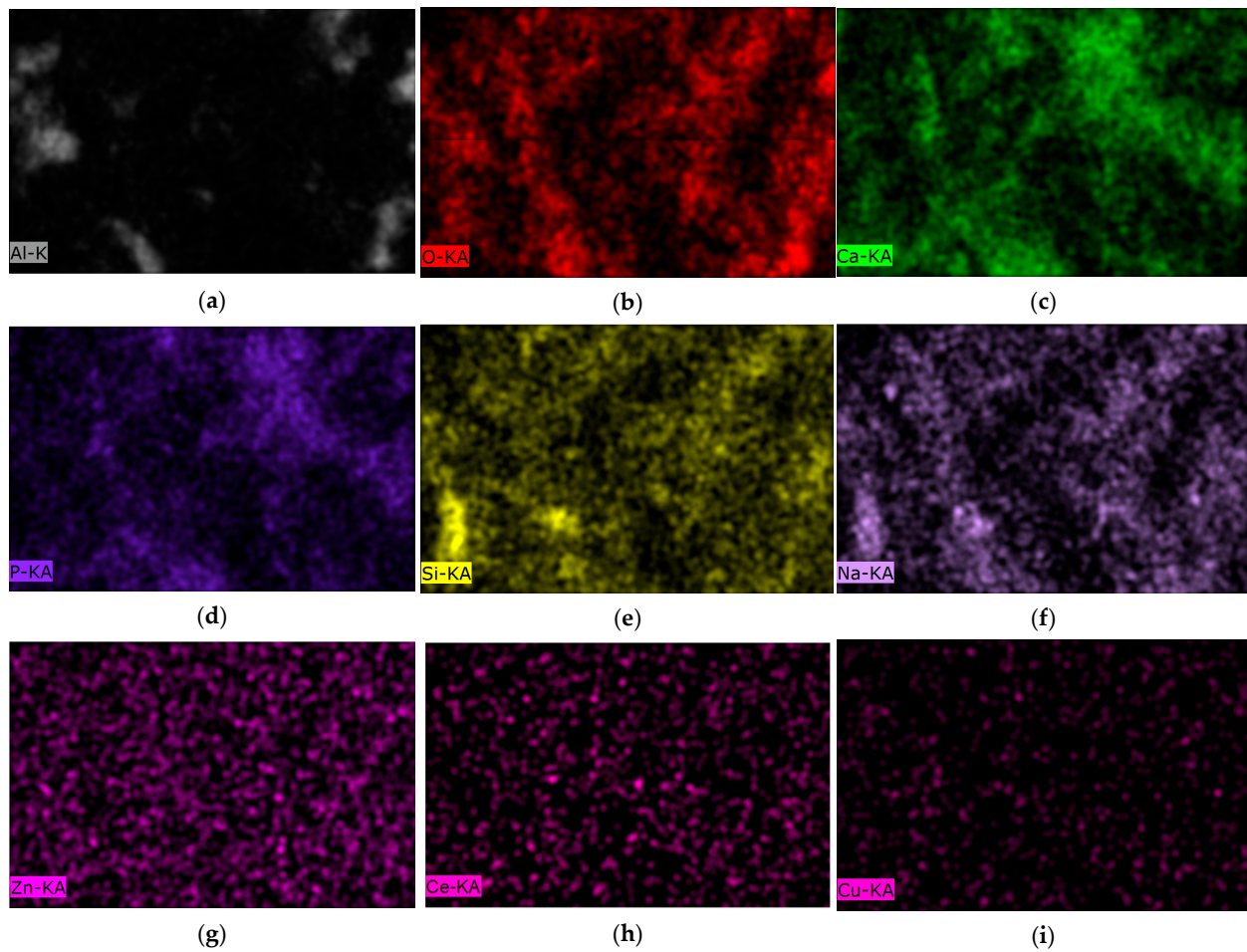


Figure 3. EDS mapping of BG/HAp samples (a–f), and sample and doping distribution of 2Zn/HAp (g), 2Ce/HAp (h), and 0.5Cu/HAp (i) (magnification: 5 kx at 15 kV).

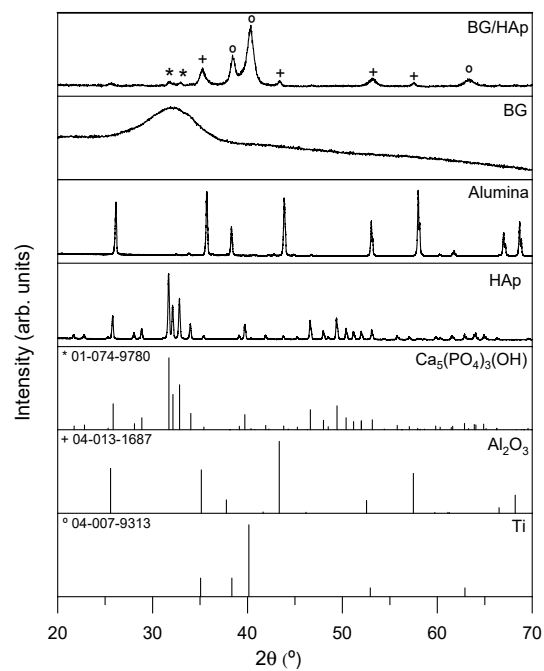


Figure 4. GIXRD of BG/HAp coating, XRD of powders (BG, Hap, and Alumina) used in CoBlast™ deposition, and peak list of $\text{Ca}_5(\text{PO}_4)_3(\text{OH})$ (ICDD: 01-074-9780), Al_2O_3 (ICDD: 04-013-1687), and Ti (IDCC: 04-007-9313).

3.2. Cell Culture

3.2.1. Cytotoxicity Assay

Cytotoxicity assays are one of the first steps in a biocompatibility assessment of a biomaterial. In this assay, the extracts obtained from the different BG/HAp coatings were placed in contact with human osteosarcoma Saos-2 cells. The cell populations were measured using the resazurin assay. The goal of this assay is to confirm that the composite coatings containing doped BG can be safely placed in contact with the organism without any harmful effects. The results obtained are presented in Figure 5.

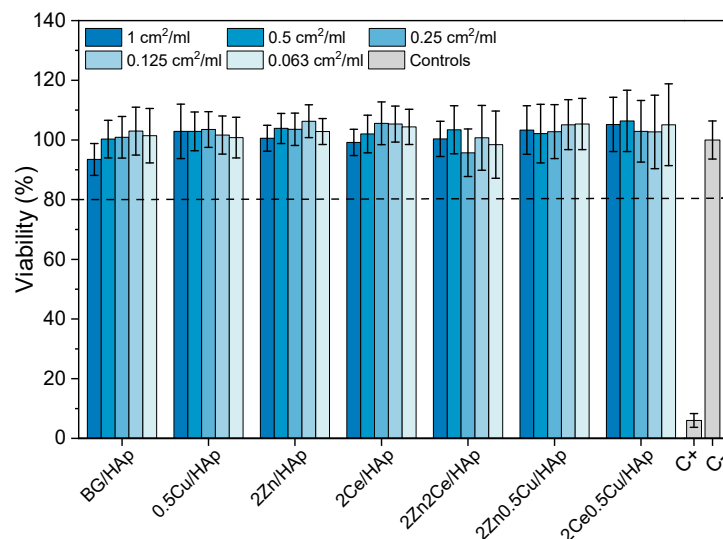


Figure 5. Relative cell viability after 48 h incubation with undoped, doped, and co-doped BG-coated sample extracts. C− is the negative and C+ is the positive control, both represented in gray. The dashed line is the minimum percentage of cell viability for which extracts are not deemed cytotoxic.

The results evidence that all tested coatings produced by CoBlast™ have relative cell viabilities above 80% in comparison with the negative control, which suggests that none of the materials tested provoked cell death and, therefore, are safe to be used as coatings for implants. The viability was as expected, since all BG powders used had already proved to be viable at concentrations up to 12.5 mg/mL for the BG, 2Ce, and 0.5Cu samples, and 50 mg/mL for the 2Zn sample [44,45,47].

The results obtained are corroborated by the findings previously described by Dias et al. where HA coatings by CoBlast™ were viable at concentrations equal or lower than 1 cm²/mL [48].

3.2.2. Adhesion and Proliferation

The adhesion and proliferation of Saos-2 cells were determined to better understand the response of bone cells to the coated implants as well as foresee their ability to assist osteointegration in vivo. The results are shown in Figure 6.

The cell adhesion assessment shows that all samples attained similar adhesion rates to the BG/HAp coating, meaning that none of the doping agents hindered the cell's ability to connect with the coating's surface. Furthermore, the 2Ce0.5Cu/HAp coating presented a significant improvement in cell adhesion.

The proliferation analysis shows a progressive increase in cell population for all samples tested. After 14 days, cells already reached the confluency stage, where there is no more available space to further proliferate. At this stage, the only factor to determinate cell populations is sample surface area. Since all coatings were produced by CoBlast™ and powders used have the same dimensions, the resulting topographies of all coated samples are similar, as was previously established in the SEM analysis, and therefore, all samples have similar final proliferation results.

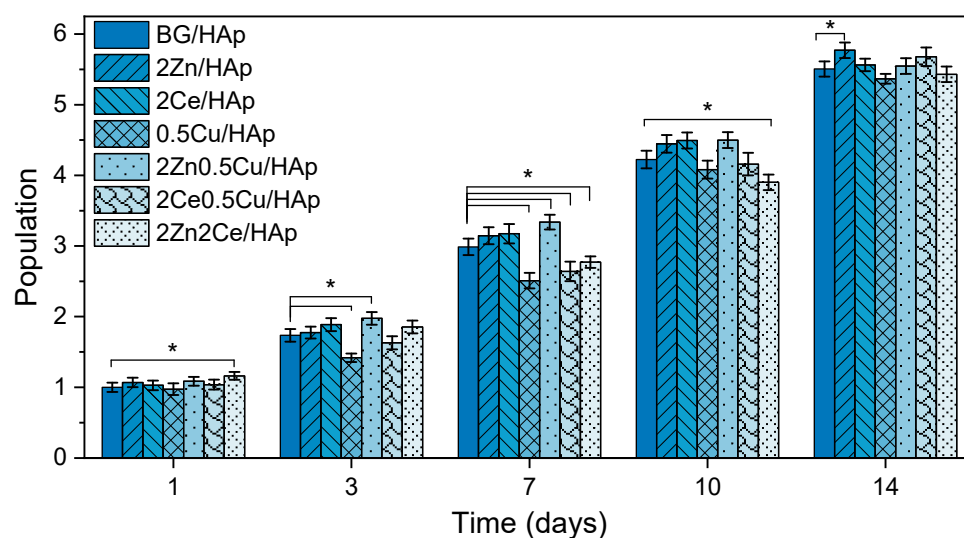


Figure 6. Comparison of populations of human osteosarcoma Saos-2 cells cultured for 14 days on all coatings. Absorbance values are normalized to the average absorbance of the BG/HAp sample on day 1. The vertical lines (whiskers) represent the standard deviation of the mean. The results of the statistical significance tests are represented with *, where $p < 0.05$.

O’Sullivan et al. [50] and Mesquita-Guimarães et al. [51] already demonstrated that cell proliferation was enhanced with coatings implementation: fibroblasts cell proliferation was studied over 7 days on Ti substrates, and Hap or BG coatings, showing a favorable response toward coated samples especially in BG samples, when compared with Ti substrates.

Cell population analysis in the first week indicated that the presence of Cu in the coatings tends to lead to worse results due to Cu’s cytotoxic behavior [45,52], which can be seen in the 0.5Cu/HAp. However, with the implementation of co-doping this effect can be mitigated with the introduction of ions with osteogenic or anti-inflammatory properties [53–55]. In this test, 2Zn0.5Cu/HAp samples presented an increase in cell population compared to the 0.5Cu/HAp coating.

Overall, all samples evidenced a favorable cell response with high human osteosarcoma Saos-2 cells, and doping agents did not jeopardize proliferation and can also improve cells responses compared to uncoated metallic implants.

3.2.3. Alkaline Phosphatase Activity

ALP is an enzyme that reflects osteoblastic activity at different stages of osteoblast differentiation. During bone regeneration there is an upregulation of ALP expression, which acts as a local concentration regulator of inorganic ions, as well as a catalyst of apatite crystals growth [56,57]. These properties lead to biomineralization and bone matrix production [58]. The relative ALP expressed by the human osteosarcoma Saos-2 cells cultured on the seven different coating throughout the 15 days of culture time is displayed in Figure 7.

All cells grown on coatings revealed an increase in relative ALP expression throughout time. However, there are no statistically significant differences between samples, not even when comparing doped sample with the BG/HAp coating. This behavior was not anticipated since Zn- [59,60] and Cu-doped [61,62] BG are supposed to increase ALP expression. The lack of statistically significant differences between samples may be due to the need to increase doping concentrations since the amount of material present in each coating is low (2 mg/cm^2), which may lead to the release of minimal amounts of doping ions with very little impact on ALP expression.

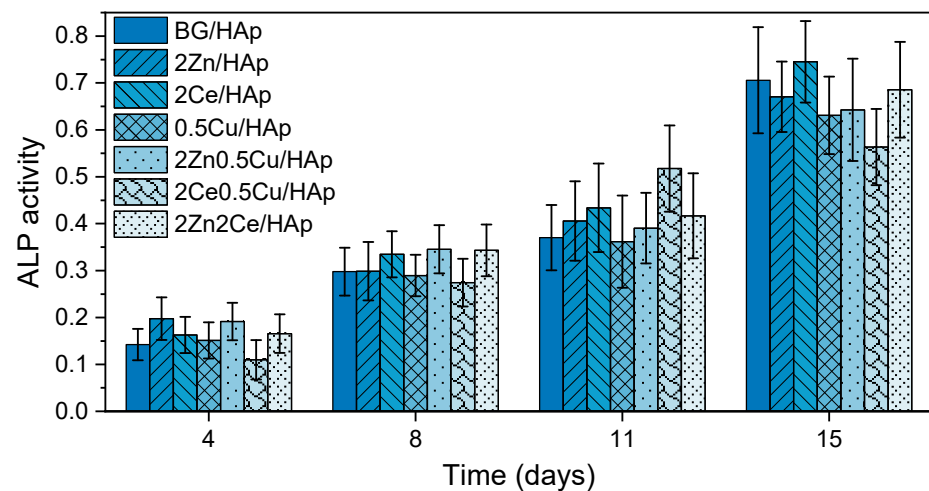


Figure 7. Relative ALP activity of human osteosarcoma Saos-2 cells on the different coatings on days 4, 8, 11, and 15. The data are normalized to the populations determined on the previous day. There are no statistically significant differences when comparing samples on each day.

3.2.4. Immunofluorescence Study

Immunofluorescence analysis is one of the most commonly used methods to study the shape, structure, size, and cell distribution on sample surfaces. For this purpose, human osteosarcoma Saos-2 cells were stained with phalloidin and DAPI to label the cytoskeleton and nuclear morphology, respectively. The cell cultures' immunofluorescence results are shown in Figure 8.

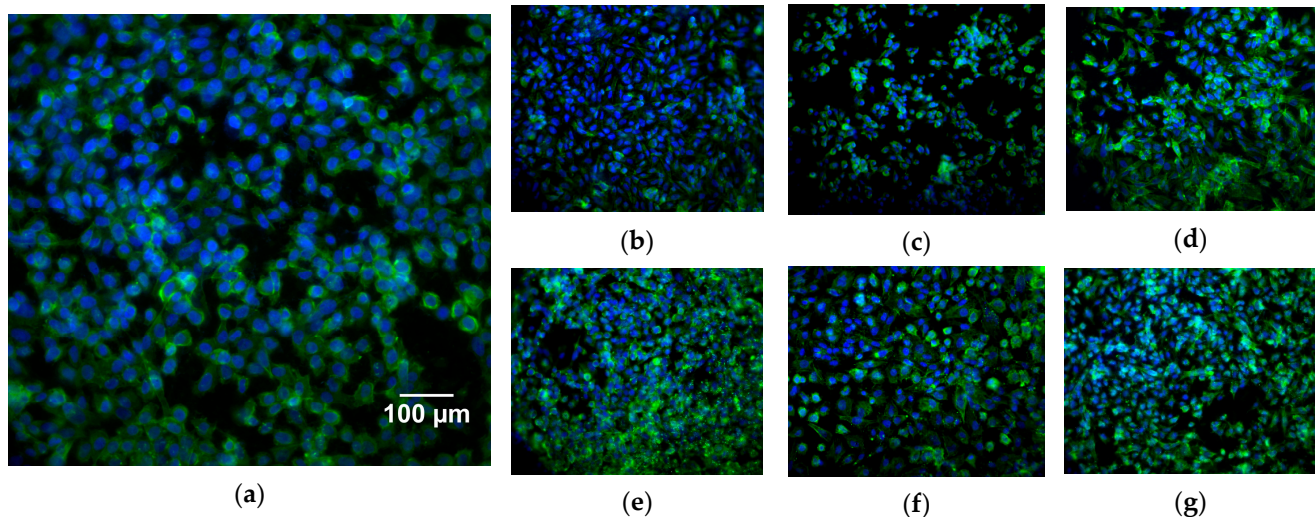


Figure 8. Immunofluorescence images after 15 days of culture of human osteosarcoma Saos-2 cells for different sample surfaces: BG/HAp (a), 2Zn/HAp (b), 2Ce/HAp (c), 0.5Cu/HAp (d), 2Zn2Ce/HAp (e), 2Zn0.5Cu/HAp (f), and 2Ce0.5Cu/HAp (g) by CoBlast™ deposition. The cytoskeleton is stained with phalloidin (green) and the nucleus is stained with DAPI (blue).

All coated samples present a high cell confluency, observable by the number of nuclei (blue dots). This fact was already expected, as it is in accordance with cell populations calculated by resazurin readings. Regarding cell morphology, the confluency stage and coating topography alters cell cytoskeleton morphology, due to spatial constraints. These spatial constraints, such as the space available for each cell, sharp edges, sharp angles, and fine textural patterns, leads to the cytoskeleton occupying a smaller area with rounded geometry that is only slightly larger than the nucleus size, instead of the polygonal or polarized fibroblastic morphology typical of Saos-2 cell line morphology [50,63].

Samples (c), (e), and (g) in Figure 8 present cells that occupy a smaller area than on other samples. These three samples have in common the presence of cerium-doped, or co-doped, bioglass. The smaller area shows that cells on these samples have a higher difficulty interacting with the surface. The cause for this is unknown and does not seem to negatively affect cell adhesion, proliferation, nor ALP production.

4. Conclusions

Several BG/Hap- and BG-doped and co-doped/HAp coatings were successfully produced by CoBlast™. All coatings presented a similar surface morphology. The in vitro response showed no cytotoxic effects, excellent proliferation, and ALP expression. Cell proliferation and immunofluorescence assays demonstrated that none of the doping agents had a negative effect on cell populations and, within 14 days, all samples reached confluency. The effect of cerium doping of cell size and morphology should be further investigated. Overall, the results reveal that BG/HAp composite coatings produced by the Coblast™ technique can improve the interaction between implants and bone for orthopedic and dental applications.

Author Contributions: Conceptualization, A.S.P. and S.R.G.; methodology, A.S.P., S.R.G., T.V. and I.H.; software, A.S.P. and S.R.G.; validation, M.P.F.G. and J.C.S.; formal analysis, A.S.P. and S.R.G.; investigation, A.S.P., S.R.G. and T.V.; data curation, A.S.P., S.R.G. and T.V.; writing—original draft preparation, A.S.P., S.R.G. and I.H.; writing—review and editing, M.P.F.G., J.C.S. and J.P.B.; supervision, J.C.S. and M.P.F.G. All authors have read and agreed to the published version of the manuscript.

Funding: FEDER funds through the COMPETE 2020 Program and National Funds through FCT—Portuguese Foundation for Science and Technology under the project LIS-BOA-01-0247-FEDER-039985/POCI-01-0247-FEDER-039985, LA/P/0037/2020, UIDP/50025/2020, and UIDB/50025/2020 of the Associate Laboratory Institute of Nanostructures, Nanomodelling, and Nanofabrication—i3N. S.R. Gavinho and A. Sofia Pádua acknowledge FCT—the Portuguese Foundation for Science and Technology for the PhD grant (SFRH/BD/148233/2019 and UI/BD/151287/2021, respectively).

Institutional Review Board Statement: Not applicable.

Informed Consent Statement: Not applicable.

Data Availability Statement: Not applicable.

Conflicts of Interest: The authors declare no conflict of interest.

References

1. Barry, J.N.; Twomey, B.; Cowley, A.; O'Neill, L.; McNally, P.J.; Dowling, D.P. Evaluation and Comparison of Hydroxyapatite Coatings Deposited Using Both Thermal and Non-Thermal Techniques. *Surf. Coatings Technol.* **2013**, *226*, 82–91. [\[CrossRef\]](#)
2. Dong, H.; Liu, H.; Zhou, N.; Li, Q.; Yang, G.; Chen, L.; Mou, Y. Surface Modified Techniques and Emerging Functional Coating of Dental Implants. *Coatings* **2020**, *10*, 1012. [\[CrossRef\]](#)
3. Joy-anne, N.O.; Su, Y.; Lu, X.; Kuo, P.H.; Du, J.; Zhu, D. Bioactive Glass Coatings on Metallic Implants for Biomedical Applications. *Bioact. Mater.* **2019**, *4*, 261–270. [\[CrossRef\]](#)
4. Guglielmotti, M.B.; Olmedo, D.G.; Cabrini, R.L. Research on Implants and Osseointegration. *Periodontology 2000* **2019**, *79*, 178–189. [\[CrossRef\]](#)
5. Liu, W.; Liu, S.; Wang, L. Surface Modification of Biomedical Titanium Alloy: Micromorphology, Microstructure Evolution and Biomedical Applications. *Coatings* **2019**, *9*, 249. [\[CrossRef\]](#)
6. Wang, Q.; Zhou, P.; Liu, S.; Attarilar, S.; Ma, R.L.W.; Zhong, Y.; Wang, L. Multi-Scale Surface Treatments of Titanium Implants for Rapid Osseointegration: A Review. *Nanomaterials* **2020**, *10*, 1244. [\[CrossRef\]](#)
7. Le Guéhennec, L.; Soueidan, A.; Layrolle, P.; Amouriq, Y. Surface Treatments of Titanium Dental Implants for Rapid Osseointegration. *Dent. Mater.* **2007**, *23*, 844–854. [\[CrossRef\]](#)
8. Gruber, R.; Bosshardt, D.D. *Dental Implantology and Implants—Tissue Interface*; Elsevier Inc.: Amsterdam, The Netherlands, 2015; ISBN 9780123977786.
9. Matos, G.R.M. Surface Roughness of Dental Implant and Osseointegration. *J. Maxillofac. Oral Surg.* **2021**, *20*, 1–4. [\[CrossRef\]](#)
10. Zhang, Y.; Chen, S.E.; Shao, J.; Van Den Beucken, J.J.P. Combinatorial Surface Roughness Effects on Osteoclastogenesis and Osteogenesis. *ACS Appl. Mater. Interfaces* **2018**, *10*, 36652–36663. [\[CrossRef\]](#)
11. Boyan, B.D.; Lotz, E.M.; Schwartz, Z. Roughness and Hydrophilicity as Osteogenic Biomimetic Surface Properties. *Tissue Eng. Part A* **2017**, *23*, 1479–1489. [\[CrossRef\]](#)

12. Kearns, V.R.; Williams, R.L.; Mirvakily, F.; Doherty, P.J.; Martin, N. Guided Gingival Fibroblast Attachment to Titanium Surfaces: An in Vitro Study. *J. Clin. Periodontol.* **2013**, *40*, 99–108. [CrossRef]
13. Dehghanghadikolaei, A.; Fotovvati, B. Coating Techniques for Functional Enhancement of Metal Implants for Bone Replacement: A Review. *Materials* **2019**, *12*, 1795. [CrossRef]
14. Prezas, P.R.; Soares, M.J.; Borges, J.P.; Silva, J.C.; Oliveira, F.J.; Graça, M.P.F. Bioactivity Enhancement of Plasma-Sprayed Hydroxyapatite Coatings through Non-Contact Corona Electrical Charging. *Nanomaterials* **2023**, *13*, 1058. [CrossRef]
15. Khan, A.A.; Al Kheraif, A.A.; Alhijji, S.M.; Matinlinna, J.P. Effect of Grit-Blasting Air Pressure on Adhesion Strength of Resin to Titanium. *Int. J. Adhes. Adhes.* **2016**, *65*, 41–46. [CrossRef]
16. Roy, M.; Vamsi Krishna, B.; Bandyopadhyay, A.; Bose, S. Laser Processing of Bioactive Tricalcium Phosphate Coating on Titanium for Load-Bearing Implants. *Acta Biomater.* **2008**, *4*, 324–333. [CrossRef]
17. Dunne, C.F.; Twomey, B.; O’Neill, L.; Stanton, K.T. Co-Blasting of Titanium Surfaces with an Abrasive and Hydroxyapatite to Produce Bioactive Coatings: Substrate and Coating Characterisation. *J. Biomater. Appl.* **2014**, *28*, 767–778. [CrossRef]
18. Tan, F.; Naciri, M.; Dowling, D.; Al-Rubeai, M. In Vitro and in Vivo Bioactivity of CoBlast Hydroxyapatite Coating and the Effect of Impact on Its Osteoconductivity. *Biotechnol. Adv.* **2012**, *30*, 352–362. [CrossRef]
19. CoBlast-ENBIO. Available online: <https://www.enbio.eu/coblast/> (accessed on 6 September 2023).
20. Dunne, C.F.; Twomey, B.; Stanton, K.T. Effect of a Blast Coating Process on the Macro- and Microstructure of Grade 5 Titanium Foam. *Mater. Lett.* **2015**, *147*, 75–78. [CrossRef]
21. Bano, S.; Romero, A.R.; Grant, D.M.; Nommeots-Nomm, A.; Scotchford, C.; Ahmed, I.; Hussain, T. In-Vitro Cell Interaction and Apatite Forming Ability in Simulated Body Fluid of ICIE16 and 13–93 Bioactive Glass Coatings Deposited by an Emerging Suspension High Velocity Oxy Fuel (SHVOF) Thermal Spray. *Surf. Coatings Technol.* **2021**, *407*, 126764. [CrossRef]
22. Jones, J.R.; Brauer, D.S.; Hupa, L.; Greenspan, D.C. Bioglass and Bioactive Glasses and Their Impact on Healthcare. *Int. J. Appl. Glas. Sci.* **2016**, *7*, 423–434. [CrossRef]
23. Jones, J.R. Reprint of: Review of Bioactive Glass: From Hench to Hybrids. *Acta Biomater.* **2015**, *23*, 53–82. [CrossRef] [PubMed]
24. Zafar, M.S.; Farooq, I.; Awais, M.; Najeeb, S.; Khurshid, Z.; Zohaib, S. *Bioactive Surface Coatings for Enhancing Osseointegration of Dental Implants*; Elsevier Ltd.: Amsterdam, The Netherlands, 2019; ISBN 9780081021965.
25. Hench, L.L. The Story of Bioglass®. *J. Mater. Sci. Mater. Med.* **2006**, *17*, 967–978. [CrossRef] [PubMed]
26. Gavinho, S.R.; Prezas, P.R.; Graça, M.P.F. Synthesis, Structural and Electrical Properties of the 45S5 Bioglass®. In *Electrical Measurements: Introduction, Concepts and Applications*; Nova Science Publisher: New York, NY, USA, 2017; ISBN 9781536129748.
27. Chitra, S.; Bargavi, P.; Balasubramaniam, M.; Chandran, R.R.; Balakumar, S. Impact of Copper on In-Vitro Biomineralization, Drug Release Efficacy and Antimicrobial Properties of Bioactive Glasses. *Mater. Sci. Eng. C* **2020**, *109*, 110598. [CrossRef] [PubMed]
28. Gavinho, S.R.; Soares, M.C.; Borges, J.P.; Silva, J.C.; Nogueira, I.S.; Graça, M.P.F. Preparation and Characterization of Zinc and Magnesium Doped Bioglasses. In *NATO Science for Peace and Security Series B: Physics and Biophysics*; Petkov, P., Achour, M.E., Popov, C., Eds.; Springer: Dordrecht, The Netherlands, 2020; pp. 465–475.
29. Zambon, A.; Malavasi, G.; Pallini, A.; Fraulini, F.; Lusvardi, G. Cerium Containing Bioactive Glasses: A Review. *ACS Biomater. Sci. Eng.* **2021**, *7*, 4388–4401. [CrossRef]
30. Shetty, S.R.; Babu, S.; Kumari, S.; Shetty, P.; Hegde, S.; Karikal, A. Status of Trace Elements in Saliva of Oral Precancer and Oral Cancer Patients. *J. Cancer Res. Ther.* **2015**, *11*, 146–149. [CrossRef]
31. Gumienna-Kontecka, E.; Rowińska-Żyrek, M.; Łuczowski, M. The Role of Trace Elements in Living Organisms. In *Recent Advances in Trace Elements*; Chojnacka, K., Saeid, A., Eds.; Wiley: New York, NY, USA, 2018; pp. 177–206.
32. Salah, I.; Parkin, I.P.; Allan, E. Copper as an Antimicrobial Agent: Recent Advances. *RSC Adv.* **2021**, *11*, 18179–18186. [CrossRef]
33. Baino, F. Copper-Doped Ordered Mesoporous Bioactive Glass: A Promising Multifunctional Platform for Bone Tissue Engineering. *Bioengineering* **2020**, *7*, 45. [CrossRef]
34. Zheng, K.; Torre, E.; Bari, A.; Taccardi, N.; Cassinelli, C.; Morra, M.; Fiorilli, S.; Vitale-Brovarone, C.; Iviglia, G.; Boccaccini, A.R. Antioxidant Mesoporous Ce-Doped Bioactive Glass Nanoparticles with Anti-Inflammatory and pro-Osteogenic Activities. *Mater. Today Bio* **2020**, *5*, 100041. [CrossRef]
35. Malavasi, G.; Salvatori, R.; Zambon, A.; Lusvardi, G.; Rigamonti, L.; Chiarini, L.; Anesi, A. Cytocompatibility of Potential Bioactive Cerium-Doped Glasses Based on 45S5. *Materials* **2019**, *12*, 594. [CrossRef]
36. Chen, Y.H.; Tseng, S.P.; Wu, S.M.; Shih, C.J. Structure-Dependence of Anti-Methicillin-Resistant Staphylococcus Aureus (MRSA) Activity on ZnO-Containing Bioglass. *J. Alloys Compd.* **2020**, *848*, 156487. [CrossRef]
37. Neščáková, Z.; Zheng, K.; Liverani, L.; Nawaz, Q.; Galusková, D.; Kaňková, H.; Michálek, M.; Galusek, D.; Boccaccini, A.R. Multifunctional Zinc Ion Doped Sol–Gel Derived Mesoporous Bioactive Glass Nanoparticles for Biomedical Applications. *Bioact. Mater.* **2019**, *4*, 312–321. [CrossRef] [PubMed]
38. Palierse, E.; Roquart, M.; Norvez, S.; Corté, L. Coatings of Hydroxyapatite-Bioactive Glass Microparticles for Adhesion to Biological Tissues. *RSC Adv.* **2022**, *12*, 21079–21091. [CrossRef]
39. Bian, T.; Wang, L.; Xing, H. Preparation and Biological Assessment of a ZrO₂-Based Bone Scaffold Coated with Hydroxyapatite and Bioactive Glass Composite. *Mater. Chem. Phys.* **2021**, *267*, 124616. [CrossRef]
40. Ielo, I.; Calabrese, G.; De Luca, G.; Conoci, S. Recent Advances in Hydroxyapatite-Based Biocomposites for Bone Tissue Regeneration in Orthopedics. *Int. J. Mol. Sci.* **2022**, *23*, 9721. [CrossRef]

41. Gavinho, S.R.; Bozdog, M.; Kalkandelen, C.; Regadas, J.S.; Jakka, S.K.; Gunduz, O.; Oktar, F.N.; Graça, M.P.F. An Eco-Friendly Process to Extract Hydroxyapatite from Sheep Bones for Regenerative Medicine: Structural, Morphologic and Electrical Studies. *J. Funct. Biomater.* **2023**, *14*, 279. [[CrossRef](#)] [[PubMed](#)]
42. Cui, W.; Yang, L.; Ullah, I.; Yu, K.; Zhao, Z.; Gao, X.; Liu, T.; Liu, M.; Li, P.; Wang, J.; et al. Biomimetic Porous Scaffolds Containing Decellularized Small Intestinal Submucosa and Sr²⁺/Fe³⁺-co-Doped Hydroxyapatite Accelerate Angiogenesis/Osteogenesis for Bone Regeneration. *Biomed. Mater.* **2022**, *17*, 025008. [[CrossRef](#)]
43. Bellucci, D.; Sola, A.; Anesi, A.; Salvatori, R.; Chiarini, L.; Cannillo, V. Bioactive Glass/Hydroxyapatite Composites: Mechanical Properties and Biological Evaluation. *Mater. Sci. Eng. C* **2015**, *51*, 196–205. [[CrossRef](#)]
44. Gavinho, S.R.; Pádua, A.S.; Sá-Nogueira, I.; Silva, J.C.; Borges, J.P.; Costa, L.C.; Graça, M.P.F. Fabrication, Structural and Biological Characterization of Zinc-Containing Bioactive Glasses and Their Use in Membranes for Guided Bone Regeneration. *Materials* **2023**, *16*, 956. [[CrossRef](#)]
45. Hammami, I.; Gavinho, S.R.; Jakka, S.K.; Valente, M.A.; Graça, M.P.F.; Pádua, A.S.; Silva, J.C.; Sá-Nogueira, I.; Borges, J.P. Antibacterial Biomaterial Based on Bioglass Modified with Copper for Implants Coating. *J. Funct. Biomater.* **2023**, *14*, 369. [[CrossRef](#)]
46. Gavinho, R.; Miguel, B.; Melo, G.; Silva, J.C.; Pedro, M.; Graça, F. Thermal, Structural, Morphological and Electrical Characterization of Cerium-Containing 45S5 for Metal Implant Coatings. *Coatings* **2023**, *13*, 294. [[CrossRef](#)]
47. Gavinho, S.R.; Pádua, A.S.; Sá-Nogueira, I.; Silva, J.C.; Borges, J.P.; Costa, L.C.; Graça, M.P.F. Biocompatibility, Bioactivity, and Antibacterial Behaviour of Cerium-Containing Bioglass[®]. *Nanomaterials* **2022**, *12*, 4479. [[CrossRef](#)] [[PubMed](#)]
48. Dias, I.J.G.; Pádua, A.S.; Pires, E.A.; Borges, J.P.M.R.; Silva, J.C.; Lança, M.C. Hydroxyapatite-Barium Titanate Biocoatings Using Room Temperature Coblating. *Crystals* **2023**, *13*, 579. [[CrossRef](#)]
49. Flanagan, J.; Schütze, P.; Dunne, C.; Twomey, B.; Stanton, K.T. Use of a Blast Coating Process to Promote Adhesion between Aluminium Surfaces for the Automotive Industry. *J. Adhes.* **2020**, *96*, 580–601. [[CrossRef](#)]
50. O’Sullivan, C.; O’Hare, P.; Byrne, G.; O’Neill, L.; Ryan, K.B.; Crean, A.M.; O’Sullivan, C.; O’Hare, P.; Byrne, G.; O’Neill, L.; et al. A Modified Surface on Titanium Deposited by a Blasting Process. *Coatings* **2011**, *1*, 53–71. [[CrossRef](#)]
51. Mesquita-Guimarães, J.; Detsch, R.; Souza, A.C.; Henriques, B.; Silva, F.S.; Boccaccini, A.R.; Carvalho, O. Cell Adhesion Evaluation of Laser-Sintered HAP and 45S5 Bioactive Glass Coatings on Micro-Textured Zirconia Surfaces Using MC3T3-E1 Osteoblast-like Cells. *Mater. Sci. Eng. C* **2020**, *109*, 110492. [[CrossRef](#)]
52. Seo, J.J.; Mandakhyar, N.; Kang, M.S.; Yoon, J.; Lee, N.-H.; Ahn, J.; Lee, H.-H.; Lee, J.; Kim, H.-W. Antibacterial, Proangiogenic, and Osteopromotive Nanoglass Paste Coordinates Regenerative Process Following Bacterial Infection in Hard Tissue. *Biomaterials* **2021**, *268*, 120593. [[CrossRef](#)]
53. Ali, A.; Ershad, M.; Vyas, V.K.; Hira, S.K.; Manna, P.P.; Singh, B.N.; Yadav, S.; Srivastava, P.; Singh, S.P.; Pyare, R. Studies on Effect of CuO Addition on Mechanical Properties and in Vitro Cytocompatibility in 1393 Bioactive Glass Scaffold. *Mater. Sci. Eng. C* **2018**, *93*, 341–355. [[CrossRef](#)]
54. Weng, L.; Boda, S.K.; Teusink, M.J.; Shuler, F.D.; Li, X.; Xie, J. Binary Doping of Strontium and Copper Enhancing Osteogenesis and Angiogenesis of Bioactive Glass Nanofibers While Suppressing Osteoclast Activity. *ACS Appl. Mater. Interfaces* **2017**, *9*, 24484–24496. [[CrossRef](#)]
55. Moghanian, A.; Ghorbanoghli, A.; Kazem-Rostami, M.; Pazhouheshgar, A.; Salari, E.; Saghafi Yazdi, M.; Alimardani, T.; Jahani, H.; Sharifian Jazi, F.; Tahriri, M. Novel Antibacterial Cu/Mg-substituted 58S-bioglass: Synthesis, Characterization and Investigation of in Vitro Bioactivity. *Int. J. Appl. Glas. Sci.* **2020**, *11*, 685–698. [[CrossRef](#)]
56. Tavares, F.J.T.M.; Soares, P.I.P.; Silva, J.C.; Borges, J.P. Preparation and In Vitro Characterization of Magnetic CS/PVA/HA/PSPIONs Scaffolds for Magnetic Hyperthermia and Bone Regeneration. *Int. J. Mol. Sci.* **2023**, *24*, 1128. [[CrossRef](#)]
57. Murray, E.; Provvedini, D.; Curran, D.; Catherwood, B.; Sussman, H.; Manolagas, S. Characterization of a Human Osteoblastic Osteosarcoma Cell Line (SAOS-2) with High Bone Alkaline Phosphatase Activity. *J. Bone Miner. Res.* **2009**, *2*, 231–238. [[CrossRef](#)] [[PubMed](#)]
58. Abe, Y.; Chiba, M.; Yakai, S.; Pechayco, R.S.; Suzuki, H.; Takahashi, T. Increase in Bone Metabolic Markers and Circulating Osteoblast-Lineage Cells after Orthognathic Surgery. *Sci. Rep.* **2019**, *9*, 20106. [[CrossRef](#)] [[PubMed](#)]
59. Cerqueira, A.; Romero-Gavilán, F.; García-Arnáez, I.; Martínez-Ramos, C.; Ozturan, S.; Iloro, I.; Azkargorta, M.; Elortza, F.; Izquierdo, R.; Gurruchaga, M.; et al. Bioactive Zinc-Doped Sol-Gel Coating Modulates Protein Adsorption Patterns and in Vitro Cell Responses. *Mater. Sci. Eng. C* **2021**, *121*, 111839. [[CrossRef](#)] [[PubMed](#)]
60. Wang, X.; Li, X.; Ito, A.; Sogo, Y. Synthesis and Characterization of Hierarchically Macroporous and Mesoporous CaO–MO–SiO₂–P₂O₅ (M = Mg, Zn, Sr) Bioactive Glass Scaffolds. *Acta Biomater.* **2011**, *7*, 3638–3644. [[CrossRef](#)]
61. Wu, C.; Zhou, Y.; Xu, M.; Han, P.; Chen, L.; Chang, J.; Xiao, Y. Copper-Containing Mesoporous Bioactive Glass Scaffolds with Multifunctional Properties of Angiogenesis Capacity, Osteostimulation and Antibacterial Activity. *Biomaterials* **2013**, *34*, 422–433. [[CrossRef](#)]
62. Zhou, Y.; Han, S.; Xiao, L.; Han, P.; Wang, S.; He, J.; Chang, J.; Wu, C.; Xiao, Y. Accelerated Host Angiogenesis and Immune Responses by Ion Release from Mesoporous Bioactive Glass. *J. Mater. Chem. B* **2018**, *6*, 3274–3284. [[CrossRef](#)]
63. Jones, S.J.; Boyde, A. Colonization of Various Natural Substrates by Osteoblasts in Vitro. *Scan. Electron Microsc.* **1979**, *2*, 529–538.

Disclaimer/Publisher’s Note: The statements, opinions and data contained in all publications are solely those of the individual author(s) and contributor(s) and not of MDPI and/or the editor(s). MDPI and/or the editor(s) disclaim responsibility for any injury to people or property resulting from any ideas, methods, instructions or products referred to in the content.